HHS Public Access

Author manuscript

J Pediatr. Author manuscript; available in PMC 2017 May 01.

Published in final edited form as:

J Pediatr. 2016 May ; 172: 14–19.e5. doi:10.1016/j.jpeds.2016.01.026.

Amino acid metabolism is altered in adolescents with NAFLD - an untargeted, high resolution metabolomics study

Ran Jin, PhD[1,*], **Sophia Banton, MS, MPH**[2,*], **ViLinh T. Tran, PhD**[2], **Juna V. Konomi, PhD**[1], **Shuzhao Li, PhD**[2], **Dean P. Jones, PhD**[2], and **Miriam B. Vos, MD, MSPH**[1]

[1]Division of Pediatric Gastroenterology, Hepatology and Nutrition, School of Medicine, Emory University, Atlanta, GA

[2]Division of Pulmonary, Allergy and Critical Care Medicine, Department of Medicine, Emory University, Atlanta, GA

Abstract

Objective—To conduct an untargeted, high resolution exploration of metabolic pathways that were altered in association with hepatic steatosis in adolescents.

Study design—This prospective, case control study included 39 Hispanic-American, obese adolescents aged 11–17 years evaluated for hepatic steatosis using magnetic resonance spectroscopy. Of these 39 individuals, 30 had hepatic steatosis ≥ 5% and 9 were matched controls with hepatic steatosis < 5%). Fasting plasma samples were analyzed in triplicate using ultra-high resolution metabolomics on a Thermo Fisher Q Exactive mass spectrometer, coupled with C18 reverse phase liquid chromatography. Differences in plasma metabolites between adolescents with and without NAFLD was determined by independent t-tests and visualized using Manhattan plots. Untargeted pathway analyses using Mummichog were performed among the significant metabolites to identify pathways that were most dysregulated in NAFLD.

Results—The metabolomics analysis yielded 9,583 metabolites, and 7,711 with 80% presence across all samples remained for statistical testing. Of these, 478 metabolites were associated with the presence of NAFLD compared with the matched controls. Pathway analysis revealed that along with lipid metabolism, several major amino acid pathways were dysregulated in NAFLD, with tyrosine metabolism being the most affected.

Conclusions—Metabolic pathways of several amino acids are significantly disturbed in adolescents with elevated hepatic steatosis. This is a novel finding and suggests that these pathways may be integral in the mechanisms of NAFLD.

Correspondence should be addressed to Dr. Miriam B. Vos; Address: Suite W450, 1760 Haygood Dr NE, Atlanta, GA, 30322; mvos@emory.edu; Phone: 404-727-9930; Fax: 404-727-4069.

*Contribed equally

The authors declare no conflicts of interest.

Keywords

tyrosine; tryptophan; methionine; branched-chain amino acids; mass spectrometry

Non-alcoholic fatty liver disease (NAFLD) has increased in prevalence and now is the most common chronic liver disease in children (1, 2). Hispanic-Americans have the highest risk of NAFLD possibly due to genetic variations, predisposition to increased adiposity, and increased exposure to high consumption of sugar-sweetened beverages (3–5). Much of our understanding of the pathogenesis of NAFLD is based upon evidence from animal models and studies in adults with NAFLD. Data in the pediatric population with NAFLD are still limited and studies exploring potential mechanisms are needed.

High resolution metabolomics is a powerful analytical tool that analyzes both individual metabolites and systemic alterations of signaling pathways for disease (6, 7). When applied as untargeted assays, high-resolution mass spectrometry can detect many endogenous metabolites, thus allowing novel discovery that is not limited to narrowly focused hypotheses. Recent advances in data extraction for ultra-high resolution mass spectrometry allow relative quantification of thousands of metabolites (8), including metabolites in 146 out of 154 known human metabolic pathways (9). A new pathway and network analysis tool used by our group and others, *Mummichog*, provides an approach for unbiased interrogation of high-resolution metabolomics data for all known metabolic pathways (10). In the current pilot study, we used these approaches in an exploratory, unbiased, untargeted metabolomics analysis of plasma samples from a group of well-matched adolescent with NAFLD and control participants to identify metabolic pathways that are dysregulated in adolescents with NAFLD.

METHODS

The study protocol was approved by the Emory University Institutional Review Board (IRB) and the Children's Healthcare of Atlanta IRB; informed consent (parental consent for participants < 18 years) and assent were obtained for each participant. Recruitment methods and inclusion/exclusion criteria have been described in detail elsewhere (11). Briefly, we recruited adolescents aged 11–18 years, self-identified as Hispanics, BMI ≥ 85th percentile for age and sex, and daily consumption of sugar-sweetened beverages > 2. Exclusion criteria included chronic alcohol consumption, previously known liver disease, any other chronic disease requiring daily medication and any acute illness and anti-oxidation therapy/supplement prior to the enrollment. Cases and controls were recruited identically and assigned into the respective categories after evaluation and completion of the magnetic resonance spectroscopy (MRS) procedure. Presence of "presumed NAFLD" (cases) was defined as MRS for hepatic steatosis ≥5% (12, 13) in combination with typical clinical history. Controls were defined as those with hepatic steatosis <5%. The MRS procedure is described in detail elsewhere (14). Participants underwent a complete history, physical exam and laboratory evaluation. Their blood samples were collected in EDTA-coated tubes after an overnight fast (at least 12 hours), processed immediately, and stored at −80°C. All participants with baseline plasma samples available were included in this analysis.

Ultra-high resolution metabolomics analysis and data processing

Frozen plasma samples were transported on dry ice to the Emory Department of Medicine Clinical Biomarkers Laboratory and maintained at −80°C until analysis. Thawed samples were processed and analyzed using liquid chromatography with ultra-high resolution mass spectrometry (LC-MS) as previously described (15). Briefly, 20 samples, along with pooled reference sample, were prepared and analyzed on a daily basis to prevent freeze/thaw cycles. For each sample, 65μL of plasma was used and acetonitrile containing a mixture of 14 stable isotope internal standards was added to the aliquot at a 2:1 ratio in order to precipitate proteins (15). The samples were kept on ice for 30 minutes and then centrifuged for 10 minutes at 13,400 × rpm at 4°C. The supernatant was then removed and placed into autosampler vials. Mass spectral data were collected with a 10-minute gradient on a Dionex UltiMate 3000 rapid separation LC system coupled with a Thermo Q Exactive MS system (Thermo Fisher Scientific, San Diego, CA). Ions were scanned in the mass-to-charge ratio (*m/z*) range from 85 to 1275 in the positive ionization mode with a resolution of 70,000. Three technical replicates were run for each sample using dual column chromatography procedure (15) with C18 chromatography (Higgins analytical, 100×2.1mm columns). Data were stored as. *raw* files and converted to computable document format (CDF) using Xcalibur file converter software (Thermo Fisher Scientific, San Diego, CA) for further processing. Following LC-MS, the data were processed using apLCMS (16) and xMSanalyzer (8) to perform peak detection, noise filtering, *m/z* and retention time alignment, and feature quantification. The metabolite values were averaged for triplicates; and data were log2 transformed and subjected to quality assessment including exclusion of data for technical replicates with overall Pearson correlation (r) < 0.70. Extraction of mass spectral data initially yielded 9,583 metabolites. Of these, 7,711 metabolites were present in > 80% of samples and were used for subsequent analysis.

Statistical Analyses

Descriptive statistics for demographic and clinical data were performed using independent t-tests or Mann-Whitney U tests (for variables without normal distribution). SEx was compared by Fisher Exact tests. The differential expression of plasma metabolites between NAFLD and controls was determined using t-tests and visualized using Manhattan plots. False discovery rate (FDR) was computed using Benjamini-Hochberg method (17), which is important in biomarker discovery where adjustments for multiple comparisons are needed to protect against FDR. For our pathway discovery analysis, we used a more conservative approach that avoided FDR error, by including all metabolites that were significant (raw p value < 0.05) and then performing statistical testing of these metabolites for pathway enrichment. The 478 significant metabolites were depicted by a heat map and subjected to pathway analysis using *Mummichog* (10), a set of algorithms specifically designed for high-throughput metabolomics. To complement univariate statistics, we also performed linear regression model, adjusted for age and sex, to test the significance of metabolite association with steatosis.

RESULTS

The demographics and clinical data of the study population are summarized in Table I. All 39 participants were obese (BMI > 95th percentile for age and sex) and self-identified as Hispanic (16 boys and 23 girls). The average age and body weight of participants was 13.8 ± 2.43 years and 80.8 ± 18.2 kilograms (mean ± SD), respectively; and hepatic steatosis ranged from 2.66% to 27.0%. Compared with controls, adolescents with ≥5% hepatic steatosis had increased liver enzymes, plasma triglycerides, insulin, as well as insulin resistance ($p < 0.05$ for all). No significant differences were observed between the two groups in terms of age, sex, body weight, BMI z-score, plasma glucose, or other lipid measurements.

Significant metabolites distinguish NAFLD from controls

To determine the metabolic differences between controls and adolescents with NAFLD, the 7,711 metabolites were analyzed by independent t-tests. Manhattan plots depict each as a function of the *m/z* and chromatographic retention time (Figure 1), with the indication of 478 metabolites above the $p < 0.05$ cutoff line. Figure 1, A shows that the metabolites vary over a broad range of molecular masses, from low mass metabolites such as metabolic intermediates to relatively high mass metabolites such as complex glycolipids. Additionally, Figure 1, B shows that many significant metabolites have retention times expected for lipophilic chemicals, e.g., fatty acids, sterols, glycerides and complex lipids. However, a relatively large fraction of the significant metabolites were eluted with characteristics of hydrophilic chemicals, such as amino acids and related metabolic intermediates.

The average intensities of the 478 metabolites are graphed in the heat map (Figure 2, A) and exhibit a clear differential expression between adolescents with NAFLD and their matched overweight controls. Table II (available at www.jpeds.com) shows *m/z*, retention time, and *p*-value of these metabolites. Representative plots for metabolites comparison between NAFLD and control groups are included in Figure 2, B-E as examples. Given the unbalanced sample size between the groups, we also analyzed the data using linear regression models to complement univariate analysis. A total of 393 *m/z* were found to significantly correlate with the severity of hepatic steatosis after adjusting for age and sex. Corresponding Manhattan plots and heat map are provided (Figures 3 and 4; available at www.jpeds.com).

Amino acid and fatty acid pathways are dysregulated in NAFLD

To explore underlying pathways dysregulated in adolescents with NAFLD, we used the software tool *Mummichog* (10) to test for significant pathways. As expected, multiple lipid metabolism pathways were affected such as *de novo* lipogenesis and fatty acid metabolism. Interestingly, a series of amino acid metabolic pathways were also dysregulated in adolescents with NAFLD (Table III). Of note, tyrosine metabolism was the most dysregulated pathway in adolescents with NAFLD. Furthermore, a strong positive association between plasma tyrosine levels and hepatic steatosis was observed even after controlling for age, sex, BMI z-score, insulin, and HOMA-IR (Table IV; available at www.jpeds.com). We also performed the pathway analysis based upon the 393 metabolites

identified by the regression model (Table III). In both models, tyrosine metabolism was the most affected pathway. Other altered amino acid pathways included branched-chain amino acids (BCAA), methionine and cysteine.

DISCUSSION

NAFLD is a multifaceted disease and known metabolic disturbances in NAFLD include upregulated *de novo* lipogenesis and elevated free fatty acids (18, 19). In our current analysis of the plasma metabolome in a group of obese, Hispanic-American adolescents, we found several amino acid metabolic pathways that were dysregulated with the presence of NAFLD. These findings are important because amino acid metabolism may serve as a novel target for the development of therapeutics for children with NAFLD.

Tyrosine metabolism was the most dysregulated pathway in adolescents with NAFLD. Previous work has provided evidence supporting the link of tyrosine metabolism with the risk for developing hyperglycemia (20), insulin resistance (21, 22), metabolic syndrome (23), and diabetes (24). Given that NAFLD is typically co-existent with insulin resistance and often co-occurs with metabolic syndrome and diabetes, it is not surprising that adolescents with NAFLD in our study exhibited dysregulation in tyrosine metabolism. In addition, we observed that plasma tyrosine levels were positively associated with the severity of steatosis in the liver, even after adjusting for age, sex, BMI z-score, and HOMA-IR. This finding is supported by a previous study analyzing frozen liver samples, which showed increased hepatic tyrosine levels in steatohepatitis when compared with simple steatosis alone (25). We expanded this observation to the pediatric population and furthered it by demonstrating an independent correlation between tyrosine levels and hepatic steatosis regardless of obesity and insulin resistance.

To date, the origins and mechanisms of tyrosine metabolism dysregulation in hepatic steatosis remain poorly elucidated. A possible explanation is that tyrosine can enter into the ketogenic pathway and be degraded directly to acetyl-CoA through ketogenesis. Therefore, high dietary tyrosine intake in the setting of calorie excess may further stimulate fatty acid synthesis and contribute to lipid deposition in the liver. It is also possible that alterations in gut microbiota, which has been seen in pediatric NAFLD (26, 27), can modulate the systemic metabolism of the host involving fatty acids and tyrosine metabolism (28) which in turn can contribute to the pathophysiology of hepatic steatosis. With the rapid expansion of “-omics”-based technology in the field of toxicology, it has been reported that derangements in tyrosine metabolism may be associated with overexposure to environmental contaminants (29, 30), such as pesticides and herbicides, that may modulate tyrosine metabolism and could potentially be involved in NAFLD pathogenesis (31).

Our data also revealed dysregulation of several other major amino acids associated with the presence of hepatic steatosis including tryptophan, branched-chain amino acids (BCAA), glycine, serine, alanine and threonine. Because liver is a critical organ for amino acid homeostasis, the imbalances could be a consequence of abnormal liver function. BCAA (leucine, isoleucine, valine) have been the most frequently investigated and observations from case control studies indicate higher BCAA levels in adults with NAFLD when

compared with age- and sex-matched controls (25, 32); however, it remains unknown whether this elevation is confounded by insulin resistance. Even though elevated plasma BCAA and its dysregulated metabolism are evident during insulin resistance and type 2 diabetes (21, 24), the role of BCAA in the pathogenesis of NAFLD, particularly in children, remains unsolved. Evidence for altered tryptophan, glycine, serine, alanine, and threonine metabolism in NAFLD is very limited and an area of future exploration.

Skeletal muscle and adipose tissue are also important regulators of amino acid metabolism and could be a source of the altered metabolism observed in this analysis. The altered levels of circulating amino acids in NAFLD might be attributed to tissue-specific dysregulation of their metabolic activities (33). We only measured the plasma metabolome in this pilot study and future studies are needed to investigate tissue-specific amino acid metabolism in patients with hepatic steatosis and fibrosis.

Strengths of the study include the untargeted approach, the huge number of metabolites identified and the well matched groups. In addition, we recruited children who had not previously been identified to have NAFLD and thus they all were in an untreated disease state providing an accurate view of the pathophysiology. There were also several limitations. The sample size was relatively small and was unbalanced between groups. We accounted for this effect using regression models but a larger control group would be helpful in future studies. This study exclusively included the Hispanic-Americans because of their high risk for NAFLD thus the findings might not be generalized to other races. We chose to compare children with NAFLD with obese, individuals without NAFLD and the pathways found differentiated NAFLD from obese without NAFLD. A normal weight, metabolically healthy, control group could be included in a future study to establish the differences from normal.

In conclusion, this exploratory metabolomics analysis demonstrated that amino acid metabolism is dysregulated in adolescents with NAFLD compared with age-, BMI-, and ethnicity-matched adolescents without evidence of significant steatosis on imaging. The alterations in amino acid metabolism, in addition to the expected upregulation of lipid metabolic pathways, is a novel finding in pediatric NAFLD. These preliminary findings suggest research is needed to explore causal links between amino acid metabolism and the pathogenesis of NAFLD and highlight the need to consider these pathways in the development of therapeutic targets for NAFLD treatment in children.

Acknowledgments

Funded by the National Institutes of Health (NIH; K23 DK080953) and the National Center for Advancing Translational Sciences of the NIH (UL1TR000454). The content is solely the responsibility of the authors and does not necessarily represent the official views of the NIH.

Abbreviations

BCAA	branched chain amino acid
LC-MS	liquid chromatography with ultra-high resolution mass spectrometry
MRS	magnetic resonance spectroscopy

NAFLD non-alcoholic fatty liver disease

References

1. Welsh JA, Karpen S, Vos MB. Increasing prevalence of nonalcoholic fatty liver disease among United States adolescents, 1988–1994 to 2007–2010. J Pediatr. 2013; 162:496–500.e1. [PubMed: 23084707]
2. Loomba R, Sanyal AJ. The global NAFLD epidemic. Nat Rev Gastroenterol Hepatol. 2013; 10:686–90. [PubMed: 24042449]
3. Schneider AL, Lazo M, Selvin E, Clark JM. Racial differences in nonalcoholic fatty liver disease in the U.S. population. Obesity (Silver Spring). 2014; 22:292–9. [PubMed: 23512725]
4. Goran MI, Walker R, Allayee H. Genetic-related and carbohydrate-related factors affecting liver fat accumulation. Curr Opin Clin Nutr Metab Care. 2012; 15:392–6. [PubMed: 22617559]
5. Vos MB, Kimmons JE, Gillespie C, Welsh J, Blanck HM. Dietary fructose consumption among US children and adults: the Third National Health and Nutrition Examination Survey. Medscape J Med. 2008; 10:160. [PubMed: 18769702]
6. Fitzpatrick AM, Park Y, Brown LA, Jones DP. Children with severe asthma have unique oxidative stress-associated metabolomic profiles. J Allergy Clin Immunol. 2014; 133:258–61.e1–8. [PubMed: 24369802]
7. Cribbs SK, Park Y, Guidot DM, Martin GS, Brown LA, Lennox J, et al. Metabolomics of bronchoalveolar lavage differentiate healthy HIV-1-infected subjects from controls. AIDS Res Hum Retroviruses. 2014; 30:579–85. [PubMed: 24417396]
8. Uppal K, Soltow QA, Strobel FH, Pittard WS, Gernert KM, Yu T, et al. xMSanalyzer: automated pipeline for improved feature detection and downstream analysis of large-scale, non-targeted metabolomics data. BMC Bioinformatics. 2013; 14:15. [PubMed: 23323971]
9. Jones DP, Park Y, Ziegler TR. Nutritional metabolomics: progress in addressing complexity in diet and health. Annu Rev Nutr. 2012; 32:183–202. [PubMed: 22540256]
10. Li S, Park Y, Duraisingham S, Strobel FH, Khan N, Soltow QA, et al. Predicting network activity from high throughput metabolomics. PLoS Comput Biol. 2013; 9:e1003123. [PubMed: 23861661]
11. Jin R, Le NA, Cleeton R, Sun X, Cruz Munos J, Otvos J, et al. Amount of hepatic fat predicts cardiovascular risk independent of insulin resistance among Hispanic-American adolescents. Lipids Health Dis. 2015; 14:39. [PubMed: 25925168]
12. Ralli EP, Rubin SH, Rinzler S. THE LIVER LIPIDS IN NORMAL HUMAN LIVERS AND IN CASES OF CIRRHOSIS AND FATTY INFILTRATION OF THE LIVER. J Clin Invest. 1941; 20:93–7. [PubMed: 16694813]
13. Lee MJ, Bagci P, Kong J, Vos MB, Sharma P, Kalb B, et al. Liver steatosis assessment: correlations among pathology, radiology, clinical data and automated image analysis software. Pathol Res Pract. 2013; 209:371–9. [PubMed: 23707550]
14. Pineda N, Sharma P, Xu Q, Hu X, Vos M, Martin DR. Measurement of hepatic lipid: high-speed T2-corrected multiecho acquisition at 1H MR spectroscopy–a rapid and accurate technique. Radiology. 2009; 252:568–76. [PubMed: 19546430]
15. Soltow QA, Strobel FH, Mansfield KG, Wachtman L, Park Y, Jones DP. High-performance metabolic profiling with dual chromatography-Fourier-transform mass spectrometry (DC-FTMS) for study of the exposome. Metabolomics. 2013; 9:132–43.
16. Yu T, Park Y, Johnson JM, Jones DP. apLCMS–adaptive processing of high-resolution LC/MS data. Bioinformatics. 2009; 25:1930–6. [PubMed: 19414529]
17. Benjamini Y, Hochberg Y. Controlling the False Discovery Rate: A Practical and Powerful Approach to Multiple Testing. Journal of the Royal Statistical Society Series B (Methodological). 1995; 57:289–300.
18. Puri P, Wiest MM, Cheung O, Mirshahi F, Sargeant C, Min HK, et al. The plasma lipidomic signature of nonalcoholic steatohepatitis. Hepatology. 2009; 50:1827–38. [PubMed: 19937697]

19. Lambert JE, Ramos-Roman MA, Browning JD, Parks EJ. Increased de novo lipogenesis is a distinct characteristic of individuals with nonalcoholic fatty liver disease. Gastroenterology. 2014; 146:726–35. [PubMed: 24316260]
20. Wurtz P, Tiainen M, Makinen VP, Kangas AJ, Soininen P, Saltevo J, et al. Circulating metabolite predictors of glycemia in middle-aged men and women. Diabetes Care. 2012; 35:1749–56. [PubMed: 22563043]
21. Wurtz P, Soininen P, Kangas AJ, Ronnemaa T, Lehtimaki T, Kahonen M, et al. Branched-chain and aromatic amino acids are predictors of insulin resistance in young adults. Diabetes Care. 2013; 36:648–55. [PubMed: 23129134]
22. Wurtz P, Makinen VP, Soininen P, Kangas AJ, Tukiainen T, Kettunen J, et al. Metabolic signatures of insulin resistance in 7,098 young adults. Diabetes. 2012; 61:1372–80. [PubMed: 22511205]
23. Wiklund PK, Pekkala S, Autio R, Munukka E, Xu L, Saltevo J, et al. Serum metabolic profiles in overweight and obese women with and without metabolic syndrome. Diabetol Metab Syndr. 2014; 6:40. [PubMed: 24650495]
24. Wang TJ, Larson MG, Vasan RS, Cheng S, Rhee EP, McCabe E, et al. Metabolite profiles and the risk of developing diabetes. Nat Med. 2011; 17:448–53. [PubMed: 21423183]
25. Lake AD, Novak P, Shipkova P, Aranibar N, Robertson DG, Reily MD, et al. Branched chain amino acid metabolism profiles in progressive human nonalcoholic fatty liver disease. Amino Acids. 2015; 47:603–15. [PubMed: 25534430]
26. Michail S, Lin M, Frey MR, Fanter R, Paliy O, Hilbush B, et al. Altered gut microbial energy and metabolism in children with non-alcoholic fatty liver disease. FEMS Microbiol Ecol. 2015; 91:1–9.
27. Vos MB. Nutrition, nonalcoholic fatty liver disease and the microbiome: recent progress in the field. Curr Opin Lipidol. 2014; 25:61–6. [PubMed: 24366230]
28. Zheng X, Xie G, Zhao A, Zhao L, Yao C, Chiu NH, et al. The footprints of gut microbial-mammalian co-metabolism. J Proteome Res. 2011; 10:5512–22. [PubMed: 21970572]
29. Lin Z, Roede JR, He C, Jones DP, Filipov NM. Short-term oral atrazine exposure alters the plasma metabolome of male C57BL/6 mice and disrupts alpha-linolenate, tryptophan, tyrosine and other major metabolic pathways. Toxicology. 2014; 326:130–41. [PubMed: 25445803]
30. Wei DD, Wang JS, Wang PR, Li MH, Yang MH, Kong LY. Toxic effects of chronic low-dose exposure of thioacetamide on rats based on NMR metabolic profiling. J Pharm Biomed Anal. 2014; 98:334–8. [PubMed: 24996005]
31. Arciello M, Gori M, Maggio R, Barbaro B, Tarocchi M, Galli A, et al. Environmental pollution: a tangible risk for NAFLD pathogenesis. Int J Mol Sci. 2013; 14:22052–66. [PubMed: 24213605]
32. Kalhan SC, Guo L, Edmison J, Dasarathy S, McCullough AJ, Hanson RW, et al. Plasma metabolomic profile in nonalcoholic fatty liver disease. Metabolism: clinical and experimental. 2011; 60:404–13. [PubMed: 20423748]
33. Cheng S, Wiklund P, Autio R, Borra R, Ojanen X, Xu L, et al. Adipose Tissue Dysfunction and Altered Systemic Amino Acid Metabolism Are Associated with Non-Alcoholic Fatty Liver Disease. PLoS One. 2015; 10:e0138889. [PubMed: 26439744]

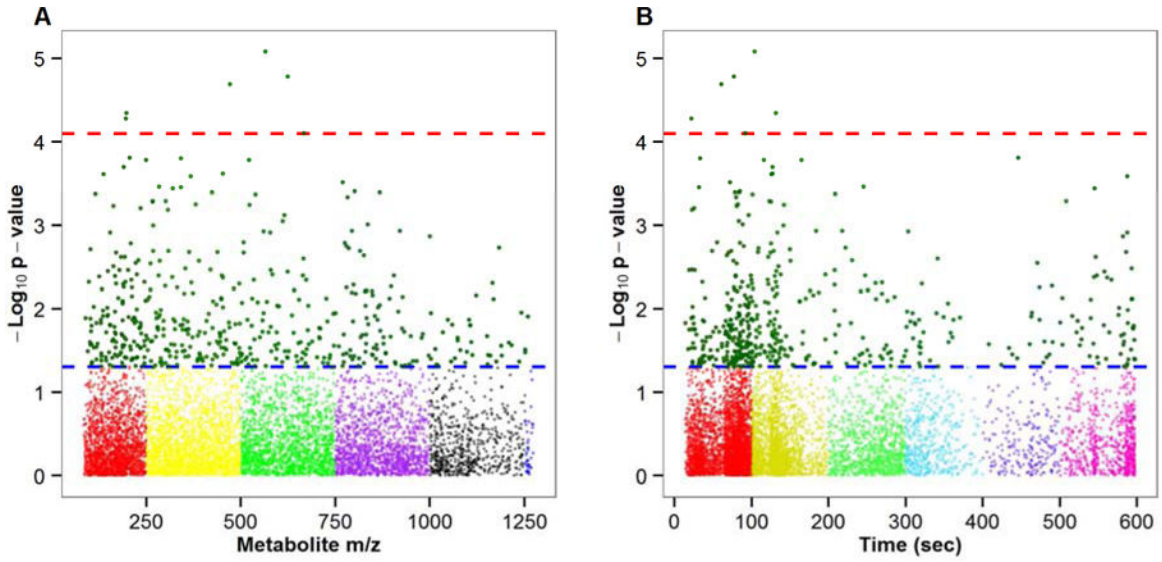

Figure 1.

Plasma metabolites that were significantly associated with the presence of hepatic steatosis. (A) Type 1 Manhattan plot showing the negative log *p* (-log p) for each metabolite (*m/z* feature) as a function of the *m/z* (mass/charge). (B) Type 2 Manhattan plot showing the -log *p* for each metabolite as a function of chromatographic retention time. The 478 statistically significant features are shown in green above the dashed blue horizontal line (raw $p < 0.05$), and all other colors are arbitrary. The red dashed line indicates false discovery rate of 0.1 (Benjamini-Hochberg correction).

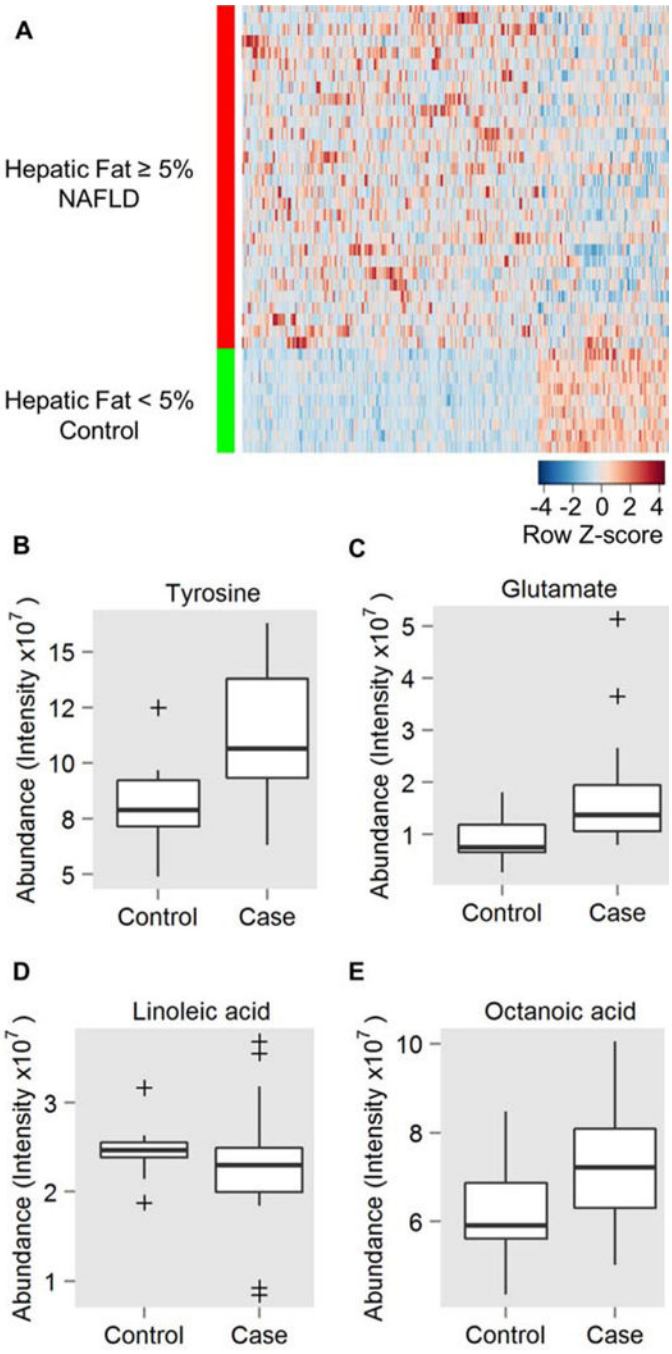

Figure 2.

(A) Heat map generated using one-way hierarchical clustering. Metabolite intensities of the significant metabolites that were differentially expressed between NAFLD and controls. Each row represents a participant and each column represents a metabolite feature. The top 478 metabolites (raw $p < 0.05$) are shown. Blue hues indicate lower intensities and red hues indicate higher intensities. (B–E) Example metabolites are shown in the box plots.

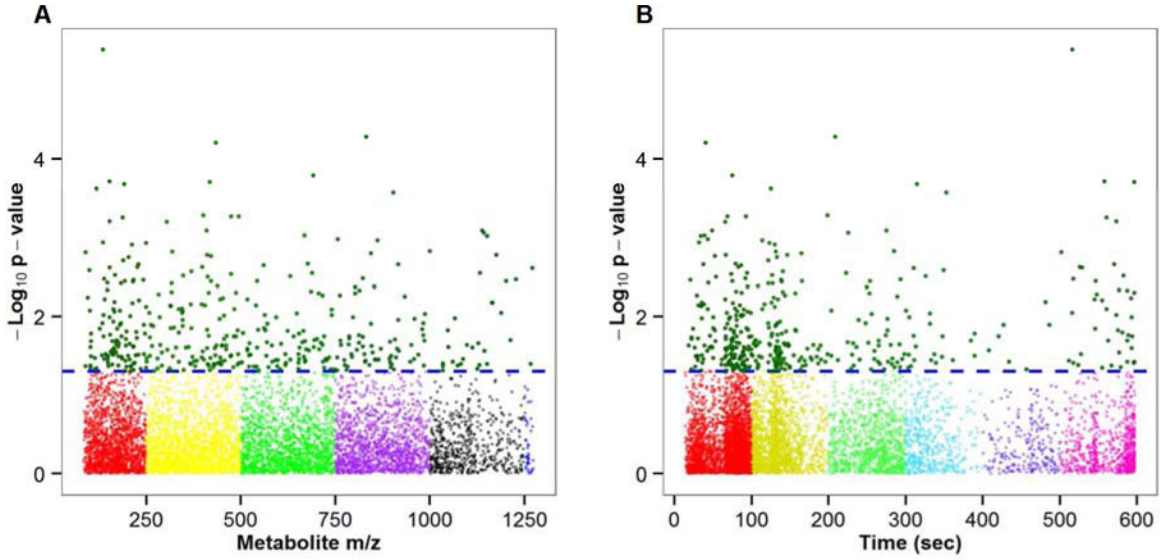

Figure 3.

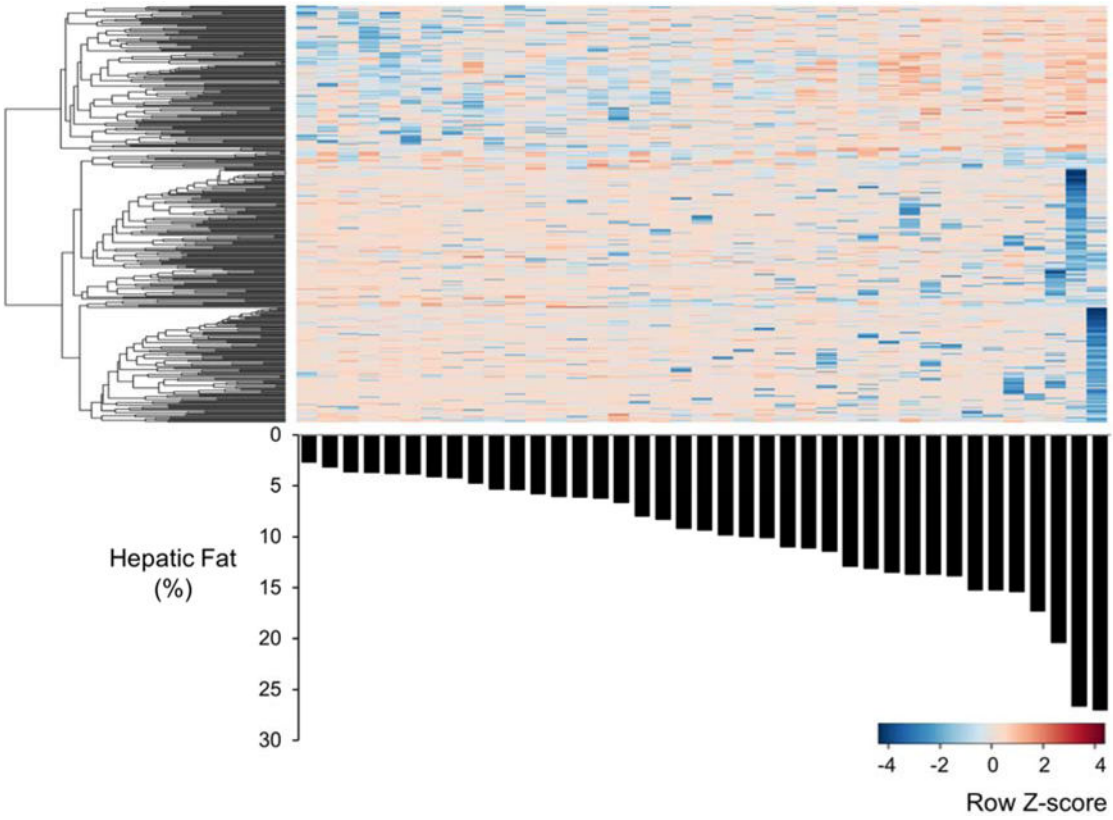

Figure 4.

Table 1

Demographic and clinical characteristics of study population.

	Total population (n=39)		Hepatic fat < 5% (n=9)	Hepatic fat ≥ 5% (n=30)
	Mean (SD)	Range		
Age, years	13.79 (2.43)	11 – 18	14.44 (2.19)	13.60 (2.50)
Male, n (%) †	16 (41.03)		3 (33.33)	13 (43.33)
Body weight (kg)	80.75 (18.18)	51.6 – 117	83.93 (23.88)	9.80 (16.48)
BMI z-score	2.06 (0.32)	1.58 – 3.42	1.97 (0.27)	2.09 (0.34)
Hepatic fat (%) *	10.1 (5.97)	2.66 – 27.0	3.75 (0.60)	11.97 (5.52)
ALT (U/L) *	35.90 (61.46)	12.0 – 398	17.33 (6.16)	41.47 (69.28)
AST (U/L) *	55.10 (161.28)	17.0 – 1035	20.33 (3.08)	65.53 (183.28)
Triglyceride (mg/dl) *	145.09 (101.04)	34.1 – 456	79.60 (30.27)	165.73 (106.75)
Cholesterol (mg/dl)	166.08 (39.39)	111 – 294	154.44 (22.58)	169.57 (42.87)
LDL (mg/dl)	105.83 (35.88)	52.9 – 221	90.89 (26.20)	110.32 (37.52)
HDL (mg/dl)	44.24 (9.30)	27.8 – 62.4	48.32 (9.59)	43.01 (9.01)
Glucose (mg/dl)	92.96 (17.54)	29.3 – 128	92.43 (18.38)	93.11 (17.61)
Insulin (mU/L) *	32.47 (26.94)	10.8 – 157	18.61 (6.57)	36.92 (29.50)
HOMA-IR *	7.75 (8.13)	1.72 – 47.7	4.17 (1.28)	8.91 (9.06)

HOMA-IR was calculated as fasting glucose (mg/dl) * insulin (mU/L)/405; Data are expressed as mean (SD).

† Values represent n (%).

* $p<0.05$ comparing children with hepatic steatosis ≥ 5% to control individuals (hepatic steatosis < 5%).

Table 2 (online only)

The m/z, retention time, and p-value for those significant 478 metabolites identified by independent t-tests (raw $p < 0.05$) comparing children with and without hepatic steatosis.

m/z	Retention Time (s)	T Statistic	raw p-value
564.6704	103.7302	5.3668	0.00001
622.9683	76.5872	5.0294	0.00002
470.2060	60.8574	5.0189	0.00002
197.0487	131.2556	4.7355	0.00004
195.0863	21.8536	4.5793	0.0001
666.5207	91.8453	−5.0373	0.0001
206.1391	446.1082	4.2328	0.0002
341.3288	32.8496	−4.2120	0.0002
249.0717	115.4367	4.3380	0.0002
521.8654	164.4972	4.2446	0.0002
190.0778	126.8233	4.1449	0.0002
452.2795	126.9677	4.0762	0.0002
136.0761	125.6614	4.3482	0.0002
367.2467	587.0451	4.0393	0.0003
768.9362	72.1495	4.0444	0.0003
283.0689	244.9569	4.0480	0.0003
341.3169	31.6208	−3.9391	0.0004
319.2759	544.8568	−3.9582	0.0004
800.6766	84.2267	−3.9731	0.0004
423.8866	78.3853	3.8950	0.0004
866.5883	83.0478	3.8940	0.0004
115.0954	208.2347	−4.2216	0.0004
538.6645	101.0162	−3.9448	0.0004
782.4976	79.6607	4.3143	0.0005
266.2485	507.9879	3.8228	0.0005
300.2000	122.9075	3.8599	0.0005
266.0387	125.0782	3.8300	0.0005
379.9297	81.5448	3.7964	0.0006
523.0735	141.5253	4.0897	0.0006
163.0365	80.6291	3.8330	0.0006
235.1805	25.2858	−3.7801	0.0006
307.1512	22.6644	4.1669	0.0006
614.5962	95.9455	−4.1692	0.0007
610.5617	83.2667	−3.6363	0.0009
834.8247	87.8251	3.6830	0.0010
267.2283	141.2739	−3.9441	0.0010
793.4005	217.3045	3.5249	0.0012
919.6810	183.4213	3.5418	0.0012

m/z	Retention Time (s)	T Statistic	raw p-value
560.1350	302.7599	−4.0643	0.0012
577.2120	587.1666	3.5064	0.0012
154.0877	133.4353	3.5124	0.0012
999.6405	581.5206	3.4846	0.0013
507.3484	54.6965	3.5058	0.0016
774.4945	84.2768	−3.9937	0.0016
209.1865	124.6240	3.4477	0.0016
778.5758	89.4459	−3.5277	0.0018
1181.7517	221.3542	−3.5491	0.0019
784.7399	108.3482	3.3549	0.0019
102.0748	149.4992	3.7123	0.0019
267.0137	128.0370	3.3788	0.0020
308.0985	73.0300	3.3762	0.0020
814.6684	48.4064	3.3197	0.0020
362.2912	585.8737	3.8226	0.0021
437.8643	107.6672	−3.7811	0.0021
507.2225	69.6853	3.3322	0.0021
170.0602	123.8347	3.4860	0.0021
825.5185	67.4989	3.2912	0.0023
182.0818	121.0438	3.5968	0.0024
193.1592	545.9001	3.2825	0.0024
665.6079	341.0599	3.2602	0.0025
229.0584	229.9666	3.2845	0.0026
388.9553	75.9072	−3.5324	0.0026
285.0705	150.6155	3.2195	0.0027
221.1907	470.1963	3.3020	0.0028
259.9968	80.3682	3.2509	0.0029
162.9115	134.8087	3.1675	0.0031
352.3007	592.7982	−3.1680	0.0033
418.2810	22.2902	−3.2473	0.0034
178.1595	18.6617	−3.1746	0.0034
579.3833	207.3417	3.1617	0.0034
201.1121	25.7369	3.1272	0.0035
148.0608	132.0117	3.1936	0.0035
623.2896	557.4474	3.4219	0.0036
223.9639	137.8016	3.0888	0.0039
583.1235	195.8330	3.0890	0.0039
282.2515	547.4747	−3.1126	0.0040
449.1595	98.6643	3.0780	0.0040
663.8577	78.8377	3.1136	0.0040
904.2113	247.4826	3.0795	0.0040
166.0648	129.5959	3.0685	0.0041

m/z	Retention Time (s)	T Statistic	raw p-value
124.8976	78.6455	−3.3973	0.0041
318.2731	544.0071	−3.1153	0.0042
452.2779	560.7656	3.0920	0.0043
672.4963	99.7173	3.2594	0.0045
534.2564	566.8856	3.0258	0.0045
210.0964	120.3541	3.0665	0.0045
194.0073	87.0393	3.0781	0.0048
245.1383	35.9803	3.0517	0.0048
98.0589	131.1315	3.0253	0.0048
368.1605	269.2046	3.0305	0.0049
1165.5730	260.4608	3.1213	0.0049
494.7287	100.0588	−3.1010	0.0050
169.9560	320.6431	2.9995	0.0050
189.0757	121.3408	3.2227	0.0051
797.6654	207.8353	3.0242	0.0052
299.9137	489.6902	2.9842	0.0053
896.7103	95.1996	2.9803	0.0054
189.5239	132.7676	−3.4619	0.0054
330.9340	76.5588	2.9842	0.0056
212.0079	473.3980	3.1674	0.0056
778.5381	85.1197	2.9454	0.0056
480.7065	101.2657	−3.4057	0.0058
132.1430	126.6855	3.0003	0.0058
260.9497	77.5716	2.9202	0.0059
640.1787	250.5106	2.9304	0.0060
833.0242	175.5403	2.9127	0.0061
828.5519	81.0809	−3.0716	0.0062
847.2484	241.6592	2.9070	0.0062
793.4369	186.8270	2.8983	0.0063
373.2334	68.3125	2.9200	0.0065
350.0669	132.7095	3.0474	0.0066
803.0938	268.8463	−3.1003	0.0066
1121.5527	179.9437	2.9618	0.0068
848.4299	90.7924	−2.9672	0.0069
211.0507	129.8802	2.8552	0.0071
258.1197	98.4465	−3.1716	0.0072
927.4948	285.2016	2.9972	0.0072
175.1381	502.8493	2.9956	0.0074
447.3486	39.2154	−2.8738	0.0074
726.0279	170.1583	2.8357	0.0075
892.5056	93.8288	2.9957	0.0075
530.3167	593.7240	2.9923	0.0075

m/z	Retention Time (s)	T Statistic	raw p-value
1167.3704	260.9473	2.8464	0.0076
447.3486	592.5028	−3.0211	0.0076
654.2286	73.7277	−3.0762	0.0078
252.9976	539.6478	2.8389	0.0078
247.0131	276.2647	2.8053	0.0080
187.1117	162.1547	2.7994	0.0081
187.1151	162.1547	2.7994	0.0081
187.1077	162.1547	2.7993	0.0081
426.7416	101.0215	−3.1152	0.0082
569.3837	117.0912	2.7965	0.0083
544.6574	96.4219	−2.8947	0.0084
502.0880	121.1091	2.8844	0.0085
186.9566	354.3669	3.1402	0.0087
435.0181	91.0522	2.7832	0.0088
866.4012	95.7060	−3.0159	0.0090
596.5350	84.6994	−2.9484	0.0091
829.4990	104.7474	2.7537	0.0092
678.9260	68.0021	−2.9025	0.0092
600.6183	93.3924	−2.9905	0.0092
111.0209	22.7036	2.8411	0.0095
451.3270	72.0344	2.7386	0.0095
862.3149	94.9421	2.7395	0.0095
145.9857	576.4479	−2.8601	0.0097
224.0917	70.6154	2.7787	0.0102
288.1240	588.1791	2.7188	0.0104
135.1019	207.5538	2.7131	0.0104
166.0549	132.5779	2.9916	0.0107
915.4584	301.4019	−3.0782	0.0108
274.8735	122.6094	2.6825	0.0111
1241.3517	463.4331	−3.1503	0.0111
560.0789	308.7494	2.7702	0.0112
1001.7593	340.1007	2.6826	0.0113
750.6704	82.7363	2.6923	0.0114
414.2700	96.0740	2.6727	0.0115
744.6495	83.6059	2.8450	0.0115
285.2059	575.9652	−2.6886	0.0118
148.0276	106.9030	2.6709	0.0119
634.5708	83.7423	3.0013	0.0119
147.0032	83.9463	2.6760	0.0121
854.6031	93.4644	2.7551	0.0121
135.0791	515.9009	−2.7470	0.0122
1259.2139	462.6762	−2.9954	0.0124

m/z	Retention Time (s)	T Statistic	raw p-value
282.2514	23.4233	−2.7987	0.0125
202.9881	348.8864	2.7443	0.0126
217.0041	369.9174	2.8815	0.0127
275.8894	21.6391	2.8837	0.0129
89.0089	539.6976	2.7272	0.0129
832.7747	80.5941	2.6544	0.0130
219.1393	99.1404	2.6275	0.0130
102.0555	106.4840	2.7922	0.0130
348.2897	99.7025	2.6131	0.0134
320.8704	129.8703	−3.0099	0.0134
860.7103	88.7020	2.5965	0.0135
1047.6533	72.5185	2.6024	0.0135
1102.7593	72.5831	2.5942	0.0135
213.0190	361.8103	2.9349	0.0136
517.2432	473.3033	2.6222	0.0136
129.0189	317.1095	−2.7428	0.0136
556.6381	101.4486	−2.7282	0.0136
187.1269	36.5466	−2.6674	0.0137
409.2809	66.1889	2.5835	0.0139
295.6430	523.1791	2.6922	0.0140
358.2783	124.1527	−2.8579	0.0142
325.3101	38.1803	2.5931	0.0142
796.1174	305.9222	2.6361	0.0142
223.0851	85.8950	2.5909	0.0142
728.4268	94.3450	2.6426	0.0142
467.8028	499.9916	−2.8821	0.0146
219.1960	587.8024	2.7175	0.0147
118.2265	14.1699	−2.6811	0.0147
129.1107	228.5618	−2.8424	0.0147
235.1544	311.3332	2.5576	0.0148
496.3116	24.2735	2.6757	0.0151
484.6121	86.3039	−2.6291	0.0153
837.2825	312.2886	2.5944	0.0154
1058.7736	69.7802	2.5504	0.0155
154.0366	128.4183	2.5373	0.0155
345.0605	74.7797	2.8200	0.0155
1105.5425	213.0835	2.6048	0.0156
339.2361	556.9816	2.5414	0.0157
1105.7749	70.1157	2.5362	0.0157
154.0593	121.0715	2.5329	0.0157
528.3095	595.9483	2.6123	0.0159
104.1362	95.5367	2.6881	0.0160

m/z	Retention Time (s)	T Statistic	raw p-value
234.1336	63.1877	2.5187	0.0163
165.5575	136.3536	2.5171	0.0164
579.1344	109.9877	2.5390	0.0165
279.1452	300.5276	2.6426	0.0166
469.3570	53.1636	2.6224	0.0166
231.1128	72.2441	2.5023	0.0169
231.1236	72.2441	2.5023	0.0169
706.5231	594.3112	−2.6764	0.0169
279.2326	528.7537	−2.6787	0.0169
425.0165	73.2281	2.5085	0.0170
926.1804	96.1400	2.5113	0.0171
710.4761	595.1054	2.5159	0.0173
295.2273	26.0998	−2.7496	0.0174
325.2382	22.0334	−2.5098	0.0175
361.1267	79.3354	2.5080	0.0175
356.3532	130.1361	−2.6332	0.0176
345.0469	75.0731	2.7016	0.0176
354.1069	25.7248	2.5636	0.0177
281.2480	19.0961	−2.6569	0.0177
676.6365	105.9327	−2.6553	0.0181
868.3215	72.5550	−2.6259	0.0182
104.0793	88.9202	2.6367	0.0185
455.1786	65.9654	−2.4705	0.0186
389.7279	49.8795	2.4962	0.0187
931.7749	166.6826	−2.7030	0.0187
557.4353	57.4045	−2.4806	0.0188
572.3731	564.0842	−2.5974	0.0190
143.9592	322.8608	2.6273	0.0191
166.0585	126.3036	2.4888	0.0191
1034.7729	67.0585	2.4558	0.0192
595.2587	521.2635	2.5426	0.0192
442.8035	110.2401	−2.7745	0.0193
639.6075	358.1871	2.5938	0.0194
404.8208	84.6725	−2.4539	0.0195
236.0414	130.6668	2.4636	0.0198
359.1523	133.0009	2.4429	0.0199
980.5823	582.5947	2.5141	0.0199
184.0734	66.8144	2.4321	0.0200
168.9048	97.3294	−2.4382	0.0200
445.3425	65.4284	2.5828	0.0201
771.9704	28.1106	2.5596	0.0204
831.4737	208.4953	−2.5600	0.0204

m/z	Retention Time (s)	T Statistic	raw p-value
186.1130	126.4227	2.4683	0.0205
820.5590	69.5054	−2.6267	0.0206
248.9767	84.2778	2.4652	0.0208
295.2273	579.7409	−2.6377	0.0208
385.9734	126.9202	2.4422	0.0210
1150.8187	144.3391	2.4890	0.0212
948.8084	69.3628	2.4292	0.0213
896.3576	94.9330	2.4412	0.0215
275.1642	46.6458	2.4013	0.0215
445.1129	84.5835	2.5032	0.0217
816.9029	77.4875	2.4308	0.0218
549.8218	41.2542	−2.7123	0.0218
191.1283	359.9311	2.4544	0.0218
877.7280	105.6176	2.3947	0.0218
707.4569	70.1211	2.4140	0.0219
371.2997	128.2872	2.3909	0.0220
1072.7817	71.8534	2.4053	0.0222
978.3208	244.0231	−2.5098	0.0223
708.1685	309.4535	−2.5163	0.0224
253.0116	131.9862	2.3856	0.0230
162.9772	82.2204	2.3981	0.0231
535.8393	527.4886	−2.4839	0.0231
196.0916	195.2546	2.5609	0.0233
461.2888	596.6725	2.5013	0.0237
1072.2832	75.2269	2.3582	0.0238
159.1133	138.4637	2.5733	0.0241
245.1020	35.4256	2.3777	0.0242
264.9431	88.3105	2.3655	0.0243
444.3689	583.2432	2.4694	0.0245
217.5729	135.0681	2.3623	0.0247
261.1315	479.8815	2.4541	0.0247
436.3647	39.8249	−2.5429	0.0247
688.5336	93.4485	−2.3405	0.0248
1108.9444	318.8944	2.5145	0.0249
657.5453	355.1619	2.3887	0.0251
170.1373	490.1952	−2.5120	0.0251
100.9176	85.1854	−2.4668	0.0252
1207.7541	68.1324	2.3462	0.0253
482.3260	23.7066	2.3981	0.0260
652.7199	94.8171	2.5767	0.0260
598.6204	98.5461	−2.5703	0.0261
416.0745	543.6826	2.4391	0.0261

m/z	Retention Time (s)	T Statistic	raw p-value
441.1670	79.3222	2.3412	0.0262
877.4990	165.9005	2.3279	0.0263
830.3651	82.5107	−2.4899	0.0263
120.0911	130.7559	2.5128	0.0263
484.7888	98.8744	−2.3791	0.0263
485.2113	61.3019	2.3238	0.0264
315.1787	460.3038	2.4885	0.0266
104.0981	93.3120	2.3594	0.0267
679.2538	407.3213	−2.5571	0.0267
323.1625	582.2947	2.4344	0.0270
102.1195	503.2219	2.3429	0.0271
858.4561	96.6583	−2.5782	0.0271
187.1441	113.0096	2.3204	0.0274
190.9464	84.5877	2.2960	0.0274
343.9646	123.0149	2.3204	0.0275
590.5899	82.2671	−2.4765	0.0275
225.1968	526.0273	2.4011	0.0275
1215.6004	274.9095	2.4501	0.0276
746.6210	104.5098	2.3966	0.0277
245.0921	37.0751	2.3033	0.0279
1188.7338	67.5009	2.2926	0.0280
759.2342	317.2024	2.2862	0.0282
207.1109	86.2525	2.3008	0.0284
118.0657	124.8134	2.4902	0.0286
365.2111	60.8906	2.2923	0.0288
447.7519	138.5800	2.2770	0.0290
110.0096	93.4538	2.2863	0.0290
167.9825	319.2683	−2.4854	0.0291
233.1563	90.5420	2.2748	0.0291
187.1481	111.3600	2.2891	0.0293
234.2052	433.6214	2.2997	0.0294
495.9385	21.9147	2.3944	0.0295
524.3022	25.6931	2.3349	0.0295
850.5132	105.4149	−2.5127	0.0297
457.0221	150.4271	2.4917	0.0297
595.2586	17.5468	2.3994	0.0302
859.3958	271.7200	2.3193	0.0306
674.4755	86.1487	−2.3594	0.0306
1014.1575	36.2651	2.2473	0.0307
460.0088	142.4104	2.2685	0.0307
208.0398	136.5522	2.3691	0.0307
305.2481	591.8352	−2.4250	0.0309

m/z	Retention Time (s)	T Statistic	raw p-value
300.1339	128.4823	2.2717	0.0311
1251.2848	152.0316	2.2727	0.0311
252.5076	55.3442	2.2392	0.0312
789.6844	46.6586	2.3040	0.0314
1079.4905	250.0460	−2.3938	0.0316
350.9880	300.2569	−2.3329	0.0317
626.9902	77.5762	2.2300	0.0322
580.5598	82.4311	−2.3528	0.0323
616.5945	100.6188	−2.3652	0.0323
345.2836	128.5798	2.3025	0.0324
309.0170	116.4402	2.3183	0.0324
95.0717	130.7708	2.2355	0.0324
328.9848	78.7879	2.2398	0.0327
1097.3191	280.2955	−2.4441	0.0330
828.8125	68.4051	2.3257	0.0331
151.1445	116.9770	2.2379	0.0332
664.4912	97.0853	−2.2183	0.0332
1251.7460	208.6278	2.2245	0.0333
183.0787	123.2713	2.3669	0.0336
497.0996	84.5807	−2.3425	0.0338
882.7310	99.9430	2.2311	0.0338
882.1906	276.8319	2.3391	0.0342
779.2546	243.8686	2.2497	0.0344
131.0709	318.8327	−2.3231	0.0344
389.3979	135.7407	2.2121	0.0344
525.2800	578.5024	−2.3808	0.0351
502.7594	111.0335	−2.3387	0.0351
670.6029	106.6893	−2.3474	0.0352
179.1436	486.2833	2.2766	0.0352
846.3419	86.9474	−2.2969	0.0354
453.0664	90.6766	2.2011	0.0354
770.6317	93.7486	−2.4255	0.0355
166.9952	438.0766	2.2501	0.0355
431.1277	86.1175	2.2018	0.0355
736.5053	90.1780	−2.3195	0.0358
1112.3215	143.4791	2.1926	0.0358
1153.3876	240.2124	2.2773	0.0359
848.3362	88.0847	−2.3620	0.0360
1158.7866	38.2660	2.1805	0.0365
391.8027	80.4556	2.1794	0.0365
1189.6000	253.7042	2.2593	0.0366
997.2397	174.1947	2.1786	0.0368

m/z	Retention Time (s)	T Statistic	raw p-value
312.1731	538.2499	−2.2384	0.0368
361.2720	67.6739	−2.1873	0.0370
131.0251	36.7777	−2.3801	0.0371
646.5170	94.1426	−2.1733	0.0371
173.1536	127.3142	2.1628	0.0371
789.2857	297.8826	−2.3643	0.0371
499.1599	146.7845	−2.4327	0.0372
799.6810	266.5944	2.1798	0.0373
351.9915	120.4191	2.2409	0.0373
436.7708	104.4612	−2.3114	0.0374
408.2583	48.7209	−2.2533	0.0378
515.1166	79.3632	−2.4550	0.0379
142.1424	44.4855	−2.1770	0.0379
226.1809	482.3806	2.1599	0.0380
193.1574	88.3561	2.1700	0.0381
328.1543	86.2151	2.1702	0.0381
245.2270	547.9524	−2.4094	0.0382
621.4725	74.6469	2.1766	0.0383
700.6511	96.8308	−2.2294	0.0384
196.9733	83.4755	−2.2640	0.0386
158.8751	82.1926	−2.3395	0.0387
720.7057	99.7494	2.2550	0.0387
223.5679	136.3991	2.1433	0.0388
623.3116	170.7596	2.1407	0.0390
1065.6865	35.2074	−2.3829	0.0391
397.2221	63.2341	−2.2183	0.0392
812.6152	44.8832	−2.1999	0.0393
734.4685	85.0038	−2.2946	0.0393
287.1005	86.1880	2.1598	0.0396
213.1104	444.6036	2.1752	0.0396
490.3903	559.4256	2.1870	0.0398
593.1501	233.4651	−2.2375	0.0399
660.4890	596.2891	−2.3013	0.0400
386.2575	44.9159	−2.2348	0.0401
1001.9471	269.8929	2.2201	0.0402
857.2710	281.3829	2.2175	0.0402
212.9999	75.1502	2.1556	0.0404
510.7562	80.5582	2.1384	0.0404
795.6106	588.3803	−2.2231	0.0404
117.1109	32.2339	2.1857	0.0407
424.2159	53.2928	−2.3126	0.0408
390.3586	596.9991	−2.1804	0.0408

m/z	Retention Time (s)	T Statistic	raw p-value
210.1349	171.0087	2.1251	0.0410
531.3522	68.0133	−2.3699	0.0413
542.9288	75.7276	2.1222	0.0413
143.0705	331.2408	2.3199	0.0416
130.0656	124.4059	2.2348	0.0421
964.5641	101.2439	2.1772	0.0421
399.3310	130.5402	2.1299	0.0422
262.5283	133.1886	2.1566	0.0423
384.8092	80.3859	2.1231	0.0424
954.7005	91.9812	2.1017	0.0425
1175.7615	38.3434	2.1111	0.0428
649.3794	64.0310	2.1271	0.0428
1235.5691	295.0008	−2.3212	0.0430
1055.6444	33.7153	2.1190	0.0433
500.3524	23.3518	2.2036	0.0434
486.7859	101.4374	−2.2061	0.0434
771.4889	31.5850	2.1101	0.0434
869.7957	253.5504	2.1737	0.0436
286.9080	76.9940	−2.2884	0.0438
906.8006	73.4232	−2.1955	0.0438
290.8561	101.3444	−2.2183	0.0438
106.0505	130.9749	2.1779	0.0438
608.6493	98.5103	−2.2439	0.0440
717.5453	199.5778	2.1056	0.0442
185.0080	478.2734	2.1532	0.0443
475.0035	75.4333	2.1681	0.0444
1093.7357	238.7050	2.1502	0.0445
671.1818	317.2536	2.1774	0.0448
729.5927	22.9846	−2.2322	0.0448
825.4069	181.9744	2.0934	0.0448
245.1285	34.8544	2.0759	0.0452
300.2620	549.8782	−2.2133	0.0452
491.1184	180.8856	−2.2224	0.0452
909.0992	223.0298	2.1000	0.0456
104.1213	94.8793	2.1200	0.0457
481.3029	586.9917	2.0889	0.0460
945.6711	69.6305	2.0744	0.0461
519.1133	75.5853	2.1122	0.0462
1152.7704	70.3388	2.0650	0.0466
491.1286	179.7062	−2.1634	0.0467
331.2096	423.8635	2.0829	0.0469
1019.4478	247.4423	−2.1895	0.0471

m/z	Retention Time (s)	T Statistic	raw p-value
153.0663	153.2820	2.1464	0.0472
1016.1720	31.0947	2.0532	0.0472
934.3890	99.7433	−2.2351	0.0475
291.0863	79.1524	2.0504	0.0477
273.0471	131.6236	−2.1688	0.0479
421.2714	50.4030	−2.1603	0.0482
811.4277	155.2491	2.0601	0.0482
924.4951	110.9436	2.0468	0.0483
537.1908	280.4257	−2.2821	0.0486
220.9603	83.6205	2.0413	0.0486
768.5556	586.8200	−2.1504	0.0487
566.2278	89.4311	2.0411	0.0488
238.2169	583.1807	2.0981	0.0492
308.9233	86.8955	2.1327	0.0492
130.1230	342.0550	−2.1568	0.0494
668.6039	100.7552	−2.0926	0.0496
161.0926	131.8532	2.0364	0.0496
189.9974	318.2937	2.1875	0.0497
266.9383	76.8595	2.0624	0.0497
741.8390	68.2700	2.0278	0.0499

Table 3

Significantly dysregulated pathways in NAFLD. The 478 significant metabolites from Student's t-test and 393 significant metabolites from regression model were used as *Mummichog* input, respectively. Only pathways with more than five hits of significant metabolites (overlap size) are shown.

Pathway	Input from t-test		Input from regression model	
	overlap size	p-value	overlap size	p-value
Tyrosine metabolism	17	<0.001	15	0.002
Fatty acid activation	9	<0.001		
de novo lipogenesis	8	<0.001		
Linoleate metabolism	6	<0.001		
Vitamin E metabolism			9	<0.001
Trypmiddlehan metabolism	10	0.001		
Glycerophospholipid metabolism	8	0.001		
Drug metabolism - cytochrome P450			8	0.002
Purine metabolism			10	0.003
Pyrimidine metabolism	7	0.003		
Glycine, serine, alanine, and threonine metabolism	7	0.013	8	0.035
Leukotriene metabolism	7	0.016		
Methionine and cysteine metabolism			7	0.020
Valine, leucine and isoleucine degradation			7	0.039

Table 4

β coefficients for the association between hepatic steatosis and plasma tyrosine levels.

Linear regression covariates	β coefficient	P value
Age, sex	0.481	0.003
Age, sex, BMI z score	0.450	0.010
Age, sex, BMI z score, HOMA-IR	0.451	0.014

HOMA-IR is an index for insulin resistance and is calculated as fasting glucose (mg/dl) * insulin (mU/L)/405.